Nonlinear Response of an Inextensible, Cantilevered Beam Subjected to a Nonconservative Follower Force

Kevin A. McHugh[1]
Department of Mechanical Engineering and Materials Science,
Duke University,
Durham, NC 27708
e-mail: kevin.mchugh@duke.edu

Earl H. Dowell
Professor
Department of Mechanical Engineering and Materials Science,
Duke University,
Durham, NC 27708
e-mail: earl.dowell@duke.edu

The dynamic stability of a cantilevered beam actuated by a nonconservative follower force has previously been studied for its interesting dynamical properties and its applications to engineering designs such as thrusters. However, most of the literature considers a linear model. A modest number of papers consider a nonlinear model. Here, a system of nonlinear equations is derived from a new energy approach for an inextensible cantilevered beam with a follower force acting upon it. The equations are solved in time, and the agreement is shown with published results for the critical force including the effects of damping (as determined by a linear model). This model readily allows the determination of both in-plane and out-of-plane deflections as well as the constraint force. With this novel transparency into the system dynamics, the nonlinear postcritical limit cycle oscillations (LCO) are studied including a concentration on the force which enforces the inextensibility constraint. [DOI: 10.1115/1.4042324]

1 Introduction

A cantilevered beam with a compressive, nonconservative follower force is known as Beck's beam problem [1]. Figure 1 illustrates the schematic of this system, where $-F_T$ is said follower force. This structure has been studied both experimentally and computationally in the literature for its interesting Hopf bifurcation behavior [2–9], and a comprehensive survey of research studies was published in 2000 [10]. Using a linear model, Beck determined that a critical force of $-\overline{F_T} = 20.05\,EI/L^2$ causes the undamped beam to become unstable. Bolotin [2,3] demonstrated via an eigenvalue approach that small visco-elastic damping values can decrease the critical force significantly, a result known for various nonconservative systems and first shown by Ziegler [11]. More recently, this system has been studied with the help of numerical methods [5–8] and the finite element method [9] to illustrate the behavior of the bifurcation as well as the nonlinear post-critical behavior of the beam. Stanciulescu et al. [9] noted that their finite element mesh needed to be highly refined to handle the dynamic analysis required to analyze the post-critical behavior.

It is interesting to note that although the Hopf bifurcation is a *nonlinear* phenomenon, most of the literature to date has focused only on *linear* stability analyses [1–3,6,9]. Luongo and D'Annibale [8,12] have performed pioneering studies into the nonlinear regime and provide a concise and insightful discussion of the state of the art. Of particular note they include work on discrete 2-bar systems such as that considered by Hagedorn to study nonlinear damping and its role on stability [13] and that of Thomsen to analyze chaos [14]. Continuous systems have been scrutinized with care as well. Crespo da Silva and Glynn [15,16] provided excellent studies with their nonlinear model derived from Hamilton's principle using a Lagrange multiplier to enforce inextensibility, the method that is utilized in this paper. They analyze stability and dynamical behavior by linearizing the equations of motion with the method of multiple time scales. Luongo et al. have contributed several notable works with their continuous beam model and multiple-scales and perturbation analyses to determine the role of damping in stability [5–8,12,17,18].

In addition to the follower force case, the nonlinear responses of the inextensible cantilevered beam subjected to free and normally forced vibrations also have been studied widely in the current literature [7,19–27], however the present mathematical model [21,24–26] has not previously been used for the follower force configuration. Recently, a nonlinear formulation was derived [26] from Hamilton's Principle to include the inextensibility of the beam, based upon the work of Novozhilov [28], which relates the in-plane and out-of-plane deflections. This model has been validated by several experimental studies which included base excitation and aeroelastic effects [25,29].

An extension of this model was developed [21] by employing a Lagrange multiplier to describe the inextensibility constraint, a method first employed by Crespo da Silva and Glynn [19,20]. This allows scrutiny of the constraint force as well as the deflections. A numerical study of this formulation using a Raleigh-Ritz expansion illustrated the nonlinear responses of beams with either cantilevered or free-free boundary conditions near resonance in response to a conventional forced excitation [24]. In this paper, the goal is to demonstrate the robustness of this same nonlinear model, expanded to explore Beck's problem. The effects of nonlinearity are again explored within this new framework for the equations of motion and their solution. The effects of linear damping are included as well. The principal focus is on the convergence of the modal series and a more in depth analysis of the

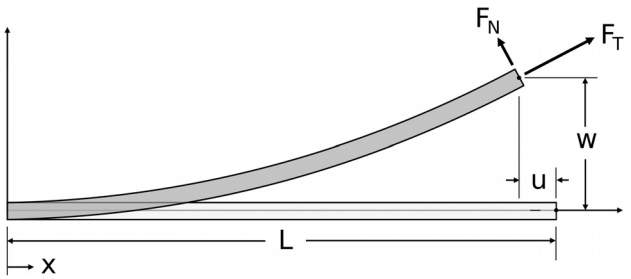

Fig. 1 Schematic of cantilever beam with follower force

[1]Corresponding author.

Contributed by the Design Engineering Division of ASME for publication in the Journal of Computational and Nonlinear Dynamics. Manuscript received September 10, 2018; final manuscript received December 5, 2018; published online January 11, 2019. Assoc. Editor: Mohammad Younis.

transverse and longitudinal deformations of the beam and the in-plane force that provides the constraint between these two planar motions.

In Sec. 2, we derive the equations of motion, beginning with the unforced system and then including the follower force. Section 3 discusses the results. We show that our model yields the published critical force of 20.05 EI/L^2 for an undamped, linear system. Further, we illustrate agreement with published results which state that adding damping to the system reduces substantially the critical force, and we briefly explore the role that damping plays in the bifurcation. For the nonlinear model, an analysis is completed of the deflection and frequency of the limit cycle oscillations (LCO), and the modal expansion of the constraint force is investigated. We then explore the importance of the number of modes in each equation of motion. It is determined that the behavior of the limit cycle oscillation requires only a small number of constraint force modes compared to longitudinal deflection modes, indicating quite interestingly that an underconstrained model is able to capture properly the dynamics of the system.

2 Methods

2.1 Unforced Governing Equations. The unforced, undamped normalized system of equations is as follows:

$$0 = L^2 m \mathbf{M_u}\ddot{\mathbf{u}} - \mathbf{A}\boldsymbol{\lambda} \tag{1}$$

$$0 = L^2 m \mathbf{M_w}\ddot{\mathbf{w}} + L^2 m\omega^2 \mathbf{M_w}\mathbf{w} + L^{-2} EI\{\mathbf{Pw}^3\} - \{\mathbf{Bw}\boldsymbol{\lambda}\} \tag{2}$$

$$0 = \mathbf{A}^{\mathbf{T}}\mathbf{u} + \frac{1}{2}\{\mathbf{Bww}\} \tag{3}$$

A full derivation is provided in Appendix A and additional detail is available in the literature [21,24]. However, it may be important to note here that Eq. (1) is the equation for longitudinal deflection u, where λ is the internal constraint force to enforce inextensibility. Equation (2) is the equation for transverse deflection w, and the final two terms are the nonlinear stiffness and inertia terms, respectively. Equation (3) is the constraint equation.

2.2 Modeling the Follower Force. The nonconservative work due to the follower force has contributions in both the u and w directions

$$\delta W^{\mathrm{NC}} = F_x \delta u|_{(x=x_F)} + F_y \delta w|_{(x=x_F)} \tag{4}$$

The follower force may have one component tangent to the axis of the beam and one component normal to the beam, respectively, F_T and F_N. So, to translate the follower force back to the x and y coordinate axes, define an angle β to be the angle of the beam at any point relative to the original undeformed horizontal axis and consider the following transformation:

$$F_x = F_T(x_F)\cos\beta(x_F) - F_N(x_F)\sin\beta(x_F) \tag{5}$$

$$F_y = F_T(x_F)\sin\beta(x_F) + F_N(x_F)\cos\beta(x_F) \tag{6}$$

Thus, the nonconservative work, δW^{NC}, can be written using Eqs. (A6), (A7), (5), (6) as

$$\delta W^{\mathrm{NC}} = (F_T(x_F)\cos\beta(x_F) - F_N(x_F)\sin\beta(x_F))\sum_i \Psi_i^u(x_F)\delta u_i + (F_T(x_F)\sin\beta(x_F) + F_N(x_F)\cos\beta(x_F))\sum_j \Psi_j^w(x_F)\delta w_j \tag{7}$$

To determine $\cos\beta$ and $\sin\beta$, we note that

$$\tan\beta = \frac{\partial w}{\partial x + \partial u} = \frac{w'}{1+u'} = \frac{w'}{1-\frac{1}{2}(w')^2} \equiv f \tag{8}$$

Using trigonometry, we may compute

$$\cos\beta = (1+f^2)^{-1/2} \tag{9}$$

$$\sin\beta = f(1+f^2)^{-1/2} \tag{10}$$

The generalized forces to be added to Eqs. (1) and (2) are identified as the coefficients of δu_i and δw_j in Eq. (7). A damping term $2L^2 m\boldsymbol{\zeta}\boldsymbol{\omega}\mathbf{M_w}\dot{\mathbf{w}}$ is added to the system in the transverse coordinate. Note that the damping coefficient $\boldsymbol{\zeta}$ is a diagonal matrix of size J^2. Two linear damping models are explored: one in which the diagonals of $\boldsymbol{\zeta}$ are held constant and one in which the diagonals of $\boldsymbol{\zeta}$ are varied such that $\boldsymbol{\zeta}\boldsymbol{\omega}$ is constant.

Finally, the system of equations including the follower forces and damping is as follows:

$$0 = L^2 m\mathbf{M_u}\ddot{\mathbf{u}} - \mathbf{A}\boldsymbol{\lambda} - (F_T(x_F)\cos\beta(x_F) - F_N(x_F)\sin\beta(x_F))\boldsymbol{\Psi}^{\mathbf{u}}(x_F) \tag{11}$$

$$0 = L^2 m\mathbf{M_w}\ddot{\mathbf{w}} + L^2 m\omega^2\mathbf{M_w}\mathbf{w} + 2L^2 m\boldsymbol{\zeta}\boldsymbol{\omega}\mathbf{M_w}\dot{\mathbf{w}} + \{\mathbf{Pw}^3\} - \{\mathbf{Bw}\boldsymbol{\lambda}\} - (F_T(x_F)\sin\beta(x_F) + F_N(x_F)\cos\beta(x_F))\boldsymbol{\Psi}^{\mathbf{w}}(x_F) \tag{12}$$

$$0 = \mathbf{A}^{\mathbf{T}}\mathbf{u} + \frac{1}{2}\{\mathbf{Bww}\} \tag{13}$$

The system of equations is solved as follows. From Eq. (11), $\ddot{\mathbf{u}}$ can be written as

$$\ddot{\mathbf{u}} = \frac{1}{L^2 m}\mathbf{M_u}^{-1}\left(\mathbf{A}\boldsymbol{\lambda} + \left(F_T(x_F)\cos\beta(x_F) - F_N(x_F)\sin\beta(x_F)\right)\boldsymbol{\Psi}^{\mathbf{u}}(x_F)\right) \tag{14}$$

Inserting this into the second time derivative of Eq. (13), we find λ in terms of w

$$\boldsymbol{\lambda} = \mathbf{A}^{-1}\boldsymbol{\Psi}^{\mathbf{u}}(x_F)F_N(x_F)\sin\beta(x_F) - \mathbf{A}^{-1}\boldsymbol{\Psi}^{\mathbf{u}}(x_F)F_T(x_F)\cos\beta(x_F) - L^2 m([\mathbf{AM_u}^{-1}\mathbf{A}]^{-1}\{\mathbf{B}\dot{\mathbf{w}}\dot{\mathbf{w}}\}) - L^2 m([\mathbf{AM_u}^{-1}\mathbf{A}]^{-1}\{\mathbf{Bww}\})\} \tag{15}$$

Here, the vectors $\{\mathbf{B}\dot{\mathbf{w}}\dot{\mathbf{w}}\}$ and $\{\mathbf{Bww}\}$ are defined as

$$\left\{\mathbf{B}\dot{\mathbf{w}}\dot{\mathbf{w}}\right\} \equiv \sum_{j_1}\sum_{j_2} B_{:j_1 j_2}\dot{\overline{w}}_{j_1}\dot{\overline{w}}_{j_2}, \quad \left\{\mathbf{Bww}\right\} \equiv \sum_{j_1}\sum_{j_2} B_{:j_1 j_2}\overline{w}_{j_1}\ddot{\overline{w}}_{j_2}$$

As expected, each term in Eq. (15) is a vector of length K and has units of force. Finally, we substitute this expression for $\boldsymbol{\lambda}$ into Eq. (12) to solve for $\ddot{\mathbf{w}}$, which provides the equation of motion for the transverse deflection. This equation is solved via a fourth-order Runge-Kutta time-marching scheme. From the solution for $\mathbf{w}$, we solve for $\mathbf{u}$ and $\boldsymbol{\lambda}$ from Eqs. (11) and (13)

$$\begin{aligned}\ddot{\mathbf{w}} = {} & (mL^2[\mathbf{BAM_uABww}] + mL^2\mathbf{M_w})^{-1}(-mL^2\omega^2\mathbf{M_w}\mathbf{w} \\ & - 2L^2 m\boldsymbol{\zeta}\boldsymbol{\omega}\mathbf{M_w}\dot{\mathbf{w}} - L^{-2}EI\{\mathbf{Pw}^3\} - mL^2\{\mathbf{BAM_uAB}\dot{\mathbf{w}}\dot{\mathbf{w}}\mathbf{w}\} \\ & + \{\mathbf{BA}\boldsymbol{\Psi}^{\mathbf{u}}\mathbf{w}\}(F_N(x_F)\sin\beta(x_F) \\ & - F_T(x_F)\cos\beta(x_F)) + F_T(x_F)\boldsymbol{\Psi}^{\mathbf{w}}(x_F)\sin\beta(x_F) \\ & + F_N(x_F)\boldsymbol{\Psi}^{\mathbf{w}}(x_F)\cos\beta(x_F))\end{aligned} \tag{16}$$

Here, several new matrices and vectors have been introduced as calculated from the tensor summations and are defined as follows:

$$[\mathbf{BAM_u ABww}] = \sum_{k_1} B_{k_1::} \sum_{k} \left(\left(\sum_{i_1} \sum_{i_2} A_{ki_1} (M^u_{i_1 i_2})^{-1} A_{i_2 k_1} \right)^{-1} \times \sum_{j_1} \sum_{j_2} B_{kj_1 j_2} \overline{w}_{j_1} \overline{w}_{j_2} \right)$$

$$\{\mathbf{BAM_u ABẇẇw}\} = \sum_{j} \sum_{k_1} B_{k_1 j:} \sum_{k} \left(\left(\sum_{i_1} \sum_{i_2} A_{ki_1} (M^u_{i_1 i_2})^{-1} A_{i_2 k_1} \right)^{-1} \times \sum_{j_1} \sum_{j_2} B_{kj_1 j_2} \dot{\overline{w}}_{j_1} \dot{\overline{w}}_{j_2} \right) \overline{w}_j$$

$$\{\mathbf{BA\Psi^u w}\} = \sum_{j} \sum_{k} B_{kj:} \sum_{i} A^{-1}_{ik} \Psi^u_i(x_F) \overline{w}_j$$

To consider the model as a linear solver, the nonlinear terms in Eqs. (11)–(13) were set to zero. Therefore, $\mathbf{u} = 0$ by Eq. (13). In addition, the expressions for $\cos\beta$ and $\sin\beta$ were redefined using small angle approximations of $\cos\beta = 1$ and $\sin\beta = \partial w/\partial x$. Therefore, from Eq. (15), we can see that $\boldsymbol{\lambda} = -\mathbf{A}^{-1}\boldsymbol{\Psi}^{\mathbf{u}}(x_F)F_T(x_F)$ for a linear Beck's Beam problem. Note that in the linear model, λ is a constant and does not depend on x or t, as it does not depend on the deflection w. This is in agreement with and can be further verified through the rigorous mathematical derivations in published literature [17,21].

2.3 Computational Methodology. For each time simulation, the beam was forced in compression with a purely tangential follower force of constant amplitude. The beam was given some small initial deflection in the first mode to displace the beam from the stable or unstable equilibrium point at zero deflection, thus biasing the system and inducing the instability when above the critical follower force. The response was calculated for a range of time, until a steady-state limit cycle was reached or until the beam deflection was sufficiently smaller than the initial displacement and showed a monotonic decrement in amplitude, indicating the response was stable and below the critical follower force.

The beam was defined to have certain material and geometric properties which were held constant for all time simulations. The beam was set to be aluminum with a modulus of elasticity of 69 GPa and a density of 2840 kg/m^3, a length of 0.508 m, a base of 0.0254 m, and a thickness of 0.0015 m.

3 Results and Discussion

3.1 Linear Model. To verify the model in the linear regime, a range of follower forces were applied to the linear, undamped model to demonstrate agreement with the known critical force of 20.05 EI/L^2. Figure 2 illustrates the tip response due to a force amplitude of 20.045 EI/L^2 versus 20.055 EI/L^2 for differing numbers of w modes.

Figure 2(*a*) shows that for a follower force below the critical force, the solution oscillates but does not decay since there is no damping in the system. (Adding damping will force the system to decay below the critical force, but it also rather interestingly changes the critical force substantially. For a damping coefficient $\zeta = 0.01$, the critical force is reduced to $\overline{F} = 16.9EI/L^2$ and the flutter frequency to 10 Hz, as will be discussed in Sec. 3.2. Note that Bolotin [2,3] has a particularly nice discussion of the effect of damping.)

For the linear model, the postcritical response is an unbounded oscillation or flutter with a flutter frequency of 14.5 Hz, as seen in Fig. 2(*b*). Note that while the deflection becomes unphysical beyond an oscillation amplitude of $w/L = 1$, the monotonic

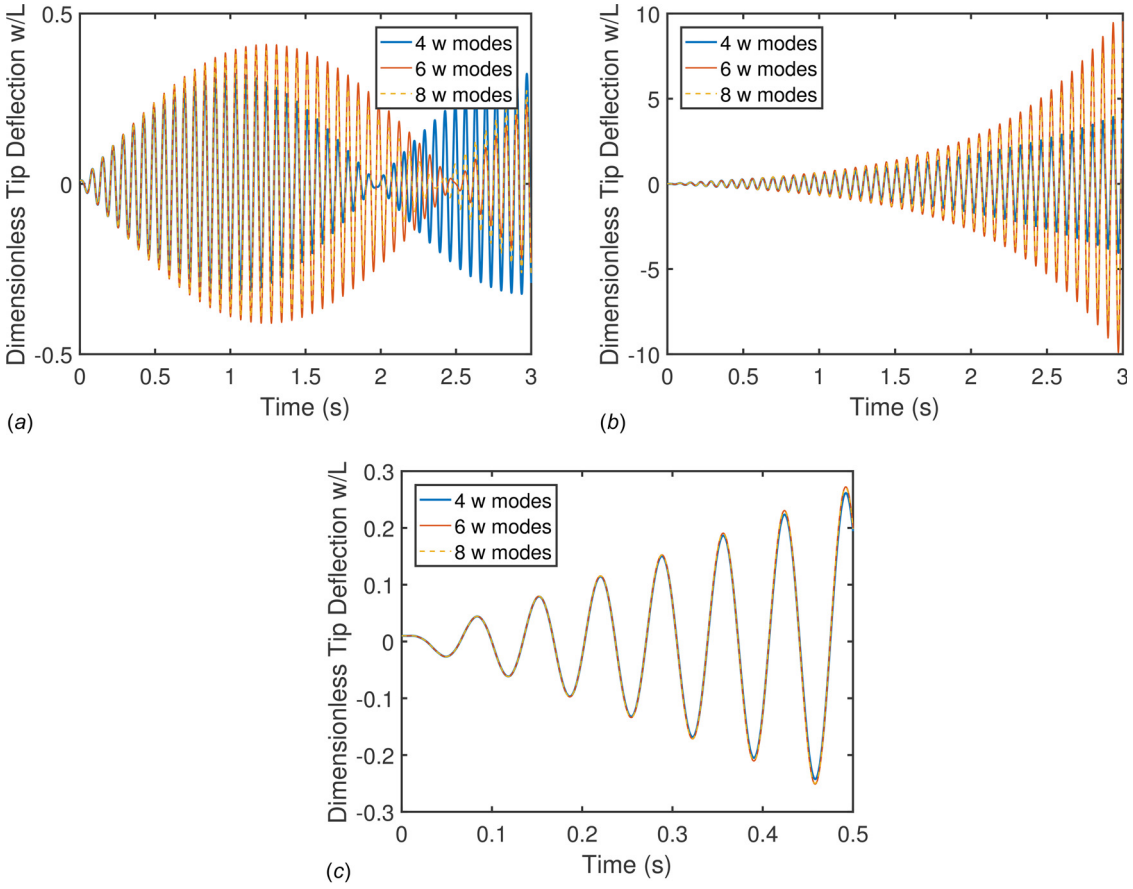

Fig. 2 Time histories for follower force of: (*a*) 20.045 and ((*b*) and (*c*)) 20.055 EI/L^2. Here (*c*) is a zoomed in plot of (*b*).

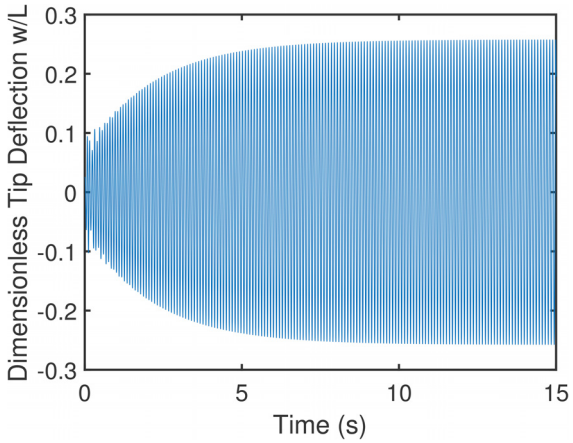

Fig. 3 Limit cycle oscillation: transverse tip deflection versus time

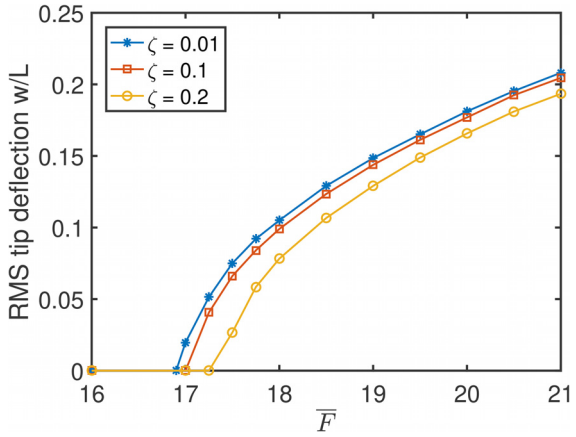

Fig. 5 RMS of transverse tip deflection versus follower force for multiple damping coefficients

increase in amplitudes depicts postcritical behavior. Figure 2(*c*) illustrates the same unbounded oscillation, but depicts a smaller range of time to demonstrate that for reasonable tip amplitudes where the linear approximations are still valid, either 4, 6, or 8 modes yield equivalent results. Modal convergence is further studied in Sec. 3.2.

3.2 Nonlinear Model. The post-critical behavior of the nonlinear model is a bounded limit cycle oscillation, as shown in Fig. 3. This figure illustrates the response of a typical case. The follower force is $\overline{F} = 20EI/L^2$, damping matrix is a constant diagonal $\zeta_{jj} = 0.01$, and there are 14 λ modes, 14 u modes, and 4 w modes. A time-step of 2×10^{-4} s was chosen after initial testing demonstrated that this would capture the behavior of the system appropriately.

Post-critical beam behavior is also investigated by performing a fast Fourier transform of the limit cycle oscillation. Figure 4 illustrates that the oscillation is a coupling of the first and second bending modes as the dominant flutter frequency of 10 Hz falls between the first and second natural frequencies, and was confirmed to be equal to the flutter frequency for the linear damped case at the flutter point. The frequency of the limit cycle oscillation increases modestly as the follower force increases beyond the instability boundary. This indicates that the instability is caused by the first two natural frequencies merging, and therefore, this behavior can be characterized as merging or coalescing frequency flutter.

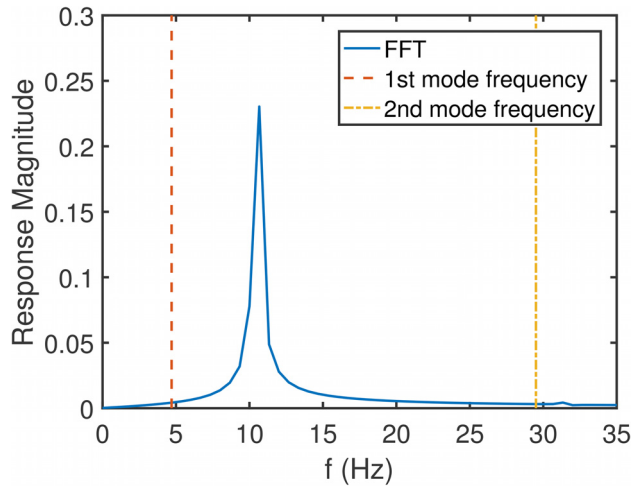

Fig. 4 Fast Fourier transform of postcritical force limit cycle (*w*/*L*) at steady-state (13.5 < *t* < 15 s)

The role of damping is briefly explored and the present results agree with published data stating that the critical force decreases with small constant damping ζ_{jj} [3]. Figure 5 illustrates that the critical force $\overline{F}$ is reduced from its undamped value of $\overline{F} = 20.05$ to values closer to $\overline{F} \approx 17$ when the diagonals of the damping matrix are held constant at $\zeta_{jj} = 0.01$. It may be noted that these values are dependent on the chosen damping model, and are not universal. In fact, Bolotin [2] showed that with constant $[\zeta\omega]_{jj}$ rather than constant ζ_{jj}, the critical force is equal to the undamped critical force. As a comparison, a case was computed with $[\zeta\omega]_{jj}$ held constant for all modes. The first modal damping coefficient was set to $\zeta_1 = 0.01$. It was determined that for this case the critical force is indeed equal to the undamped case of $\overline{F} = 20.05$, and that the flutter frequency is 14.5 Hz, again equal to the linear undamped flutter frequency. This slight increase in flutter frequency from the constant ζ_{jj} model is expected as the higher modes are more lightly damped. Further effects of chosen damping models have been presented by Luongo and D'Annibale [8], D'Annibale et al. [18] and Kirillov and Seyranian [30]. Additionally, Raviv Sayag and Dowell [25] suggested a nonlinear aerodynamic damping model for this system may be necessarily based on the experimental results. Although the study of damping is interesting, it is not the primary focus of this paper, and the constant ζ_{jj} model is used as representative and typical.

A novelty of the current model is the modal expansion of each component of the deflections u and w as well as the constraint force λ. In this regard, the nonlinear model has more subtleties than the linear model. For the linear case, one may ignore the u motion and consider only a single λ mode, because λ does not vary with x (or t). However, for the nonlinear model, the values of λ and u are no longer constants, but vary with x and t. Therefore, all three components must demonstrate modal convergence. Figure 6 illustrates the modal contributions of each component, all normalized to the maximum modal coefficient. These contributions are generated from the root-mean-square (RMS) of each mode's response for the case illustrated in Fig. 3.

To further demonstrate modal convergence, Figs. 7–9 illustrate the tip deflection behavior with respect to the number of modes in each generalized coordinate. Figure 7 shows the variation of tip deflection with respect to the number of u and λ coordinates. Note the number of u modes must be greater or equal to the number of λ coordinates to avoid an over constrained system. It can be seen that the solution is well converged with five modes in u and λ. Note that in Fig. 6(*a*) the last modal coefficient is slightly larger than the previous coefficient. Thus, even though the solution is well-converged overall, the highest modal coefficients may not be accurately determined whatever the total number of modes employed in the computation.

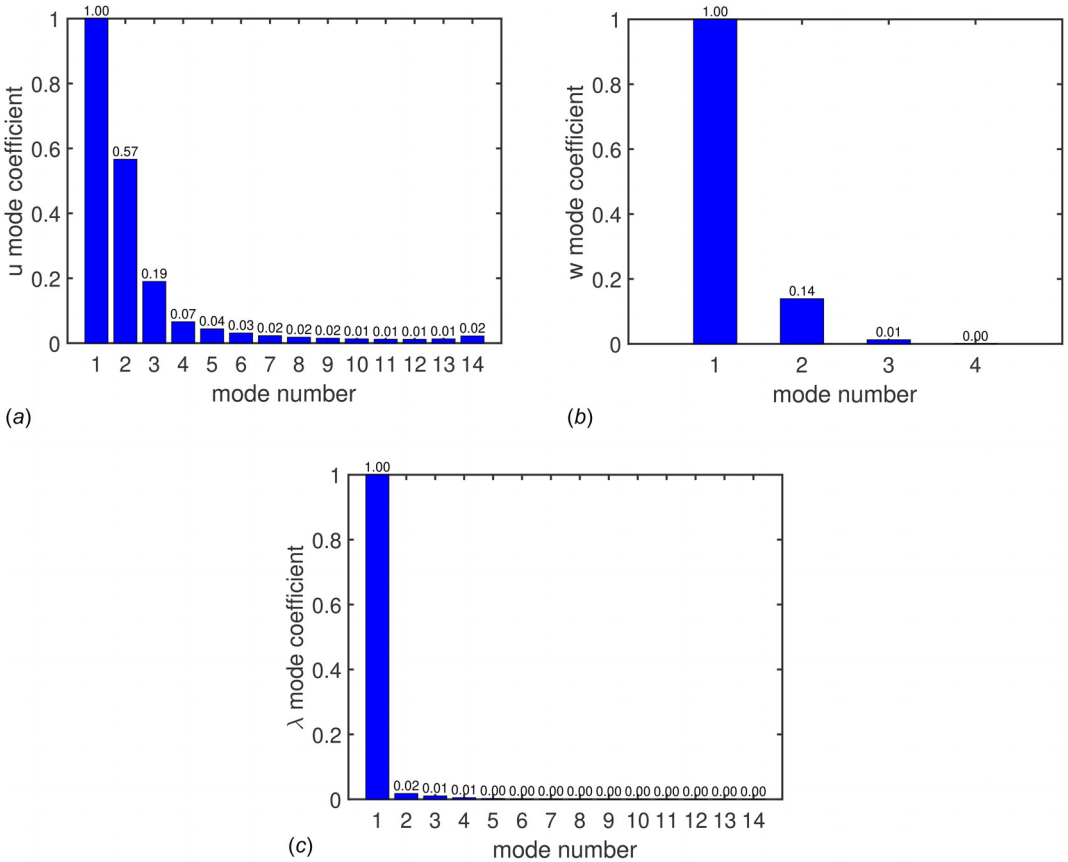

Fig. 6 Modal convergence of (*a*) *u* modes, (*b*) *w* modes, and (*c*) λ modes

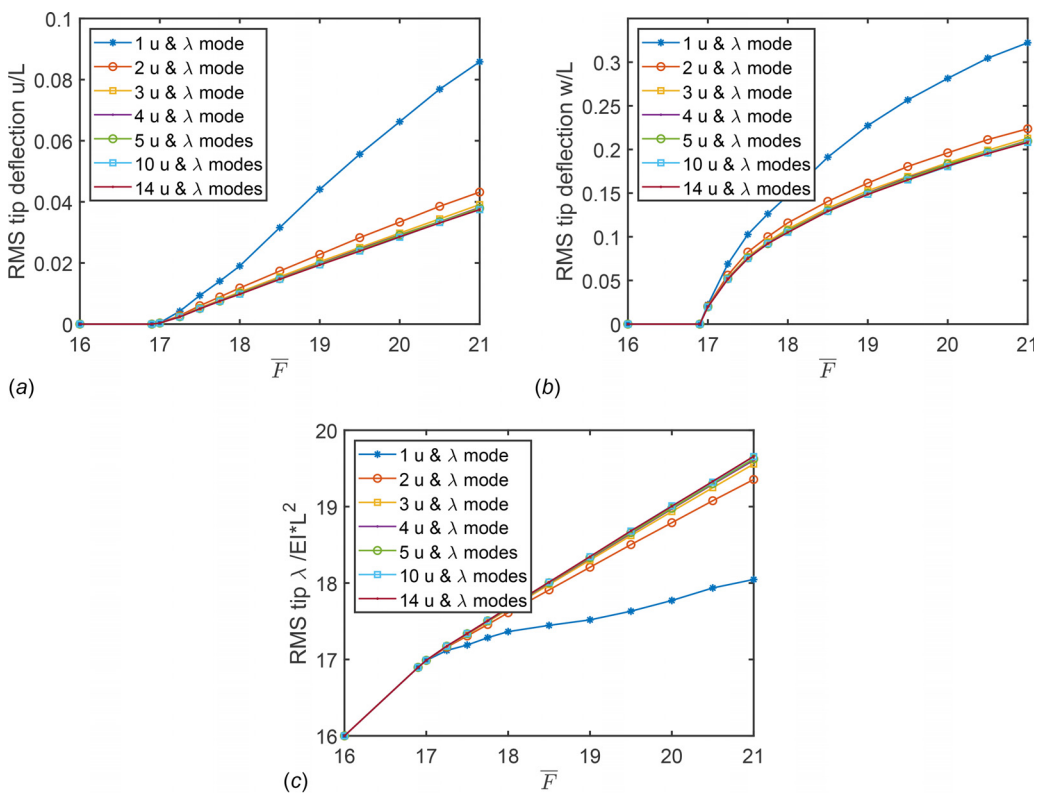

Fig. 7 RMS tip deflection in (*a*) *u* and (*b*) *w* and (*c*) RMS λ at tip versus follower force with varying numbers of *u* and λ modes

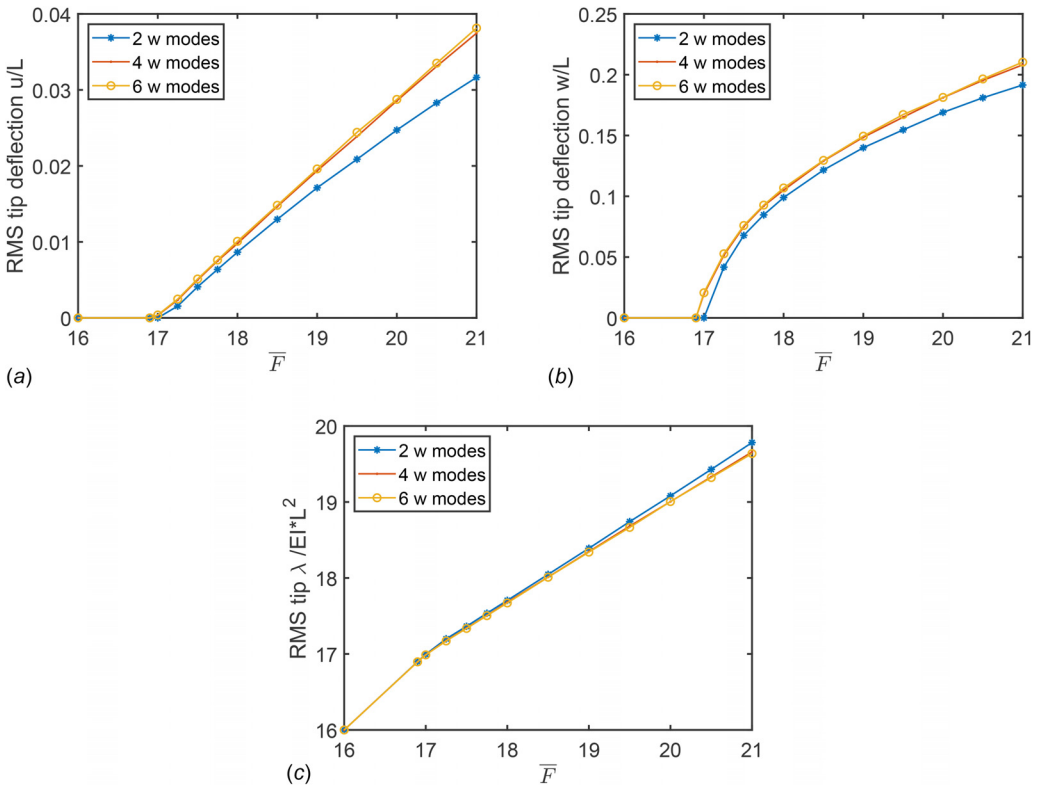

Fig. 8 RMS tip deflection in (*a*) *u* and (*b*) *w* and (*c*) RMS λ at tip versus follower force with varying numbers of *w* modes

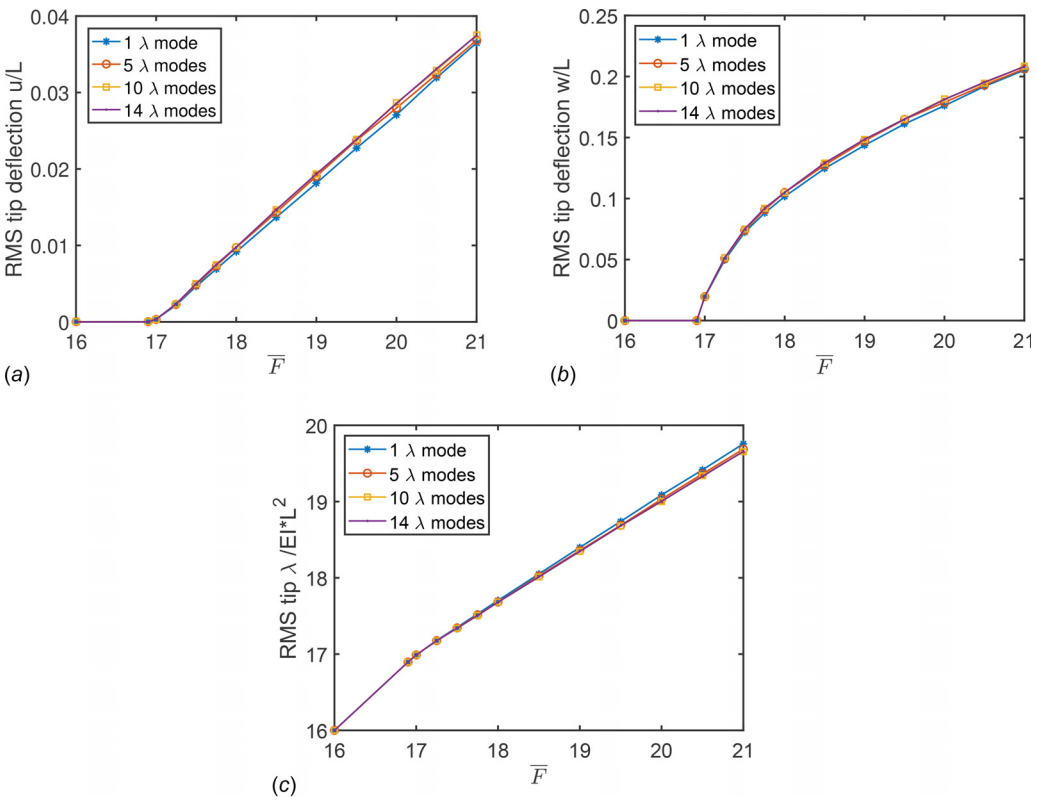

Fig. 9 RMS tip deflection in (*a*) *u* and (*b*) *w* and (*c*) RMS λ at tip versus follower force with varying numbers of λ modes

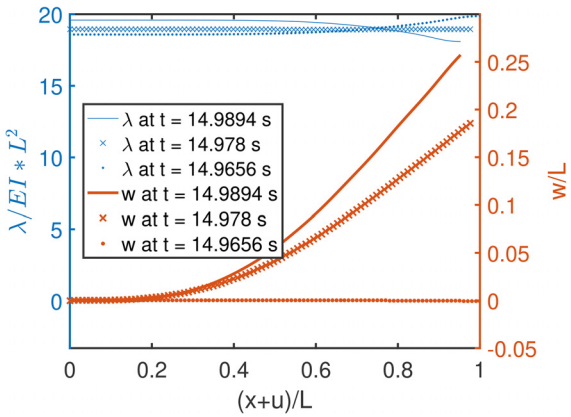

Fig. 10 Distribution of λ values across beam at corresponding beam deflections

Figure 8 shows a similar plot but for the number of w modes. Only even numbers of modes are considered because the even and odd modes couple and therefore they are best considered in tandem. It is clearly seen that the solution is converged at four modes in w.

Figure 6(*c*) illustrates that λ reaches modal convergence quickly, but it is important to note that the first mode in λ is the rigid body mode. Interestingly, Fig. 9 shows that if the system is solved with fewer λ modes than u modes—an underconstrained system—the results are acceptable for the response in each component.

To further understand this phenomenon, Fig. 10 illustrates the manner in which λ relates to the beam deflection as the beam responds to the follower force case of Fig. 3. The bold curves show the beam deflection (marked on the right axis) and thin curves near the top of the figure represent λ distribution (marked on the left axis). Three points in time are shown to illustrate how the internal force is related to the beam deflection. Interestingly, when the beam deflection is zero (marked by dotted lines), the distribution of λ is not constant, but at the tip is equivalent to the follower force amplitude. The lines marked by x's show when the internal force is constant. Finally, the solid lines show when the beam is at maximum deflection. Note that for these two deflected cases, the internal force at the tip is equal to the applied force scaled by $\cos\beta$ at the tip. Overall, λ is nearly constant and as shown in Fig. 9, not many λ modes are needed to capture the LCO behavior, since the first mode is dominant, especially at lower follower force amplitudes.

4 Conclusions

A nonconservative follower force has been applied to a contemporary, nonlinear, inextensible cantilever beam model. The governing equations were derived from the Lagrange Equations, and were expanded modally using the Raleigh-Ritz method. The results show new insight into the post-critical nonlinear characteristics of Beck's beam problem, including the behavior of the constraint force acting to relate transverse and longitudinal deflections.

The critical follower force was determined via a fourth-order Runge-Kutta time-marching solver to be the same as that previously published. The results from two commonly used linear damping models were compared. It was found that one damping model decreased the critical follower force substantially, while the other did not.

Post-critical nonlinear behavior was analyzed, and it was shown to be a limit cycle oscillation due to a merging frequency flutter mechanism as indicated by the coupling of the first and second bending modes.

The constraint force that enforces inextensibility was analyzed and shown to be correlated to the applied follower force scaled by the angle of the tip during the limit cycle oscillations. It was shown that the modal series of λ converged rather quickly and the number of λ modes can be few to compute accurately the limit cycle amplitude in either u or w.

Acknowledgment

The work of the first author was funded by a Department of Defense SMART Fellowship.

The authors would like to thank the reviewers for several insightful comments and suggestions that have helped improve the paper.

Funding Data

- Department of Defense SMART Scholarship.

Nomenclature

EI = beam bending stiffness
f = constraint function
F = force applied
$\overline{F}$ = normalized follower force applied
L = beam length
m = mass per unit length of beam
T = kinetic energy
u = longitudinal (in-plane) deflection
V = potential energy
w = transverse (out-of-plane) deflection
W^{NC} = nonconservative work
x = spatial coordinate
x_F = location of applied force
β = angle of beam with respect to horizontal
δ = virtual change operator
λ = Lagrange multiplier
Ψ = mode shape
$\mathcal{L}$ = Lagrangian
$\dot{}$ = denotes time derivative

Appendix: Derivation of Unforced Equations of Motion

To derive the equations of motion, we use the Lagrange equations for the transverse (w) and longitudinal (u) coordinates, as well as the Lagrange multiplier λ which enforces the inextensibility constraint. The Lagrange equations are

$$\frac{\partial}{\partial t}\left(\frac{\partial \mathcal{L}}{\partial \dot{q}_n}\right) - \frac{\partial \mathcal{L}}{\partial q_n} = Q_n \tag{A1}$$

where

$$\mathcal{L} = T - V + \int_0^L \lambda f \, dx \tag{A2}$$

$$T = \frac{1}{2}\int_0^L m[\dot{u}^2 + \dot{w}^2]\, dx \tag{A3}$$

$$V = \frac{1}{2}\int_0^L EI\left(\frac{\partial^2 w}{\partial x^2}\right)^2 \left[1 + \left(\frac{\partial w}{\partial x}\right)^2\right] dx \tag{A4}$$

$$f = \frac{\partial u}{\partial x} + \frac{1}{2}\left(\frac{\partial w}{\partial x}\right)^2 = 0 \tag{A5}$$

Now, the deflections and the Lagrange multiplier, u, w, and λ, are expressed in terms of modal expansions as follows:

$$u(x,t) = \sum_i \Psi_i^u(x) u_i(t) \tag{A6}$$

$$w(x,t) = \sum_j \Psi_j^w(x) w_j(t) \tag{A7}$$

$$\boldsymbol{\lambda}(x,t) = \sum_k \Psi_k^{\lambda}(x) \lambda_k(t) \tag{A8}$$

The mode shapes Ψ are chosen to satisfy the geometric constraints, i.e., $u = w = (\partial w/\partial x) = 0$ for a clamped end.

The mode shapes for u, w, and λ for the cantilevered beam are chosen to be

$$\Psi_i^u = \sin\left(\frac{2i-1}{2}\pi\xi\right) \quad \text{for} \quad i = 1, 2, 3\ldots \tag{A9}$$

$$\Psi_j^w = \frac{1}{2}\left(\cosh\left(\eta_j L\xi\right) - \cos\left(\eta_j L\xi\right) + R_j \sin\left(\eta_j L\xi\right) - R_j \sinh\left(\eta_j L\xi\right)\right) \quad \text{for} \quad j = 1, 2, 3\ldots \tag{A10}$$

$$\Psi_k^{\lambda} = \cos(k\pi\xi) \quad \text{for} \quad k = 0, 1, 2\ldots \tag{A11}$$

where η_j and R_j are determined from the cantilevered classical linear eigenvalue equation

$$0 = \cos(\eta_j L)\cosh(\eta_j L) + 1 \tag{A12}$$

$$R_j = (\cosh(\eta_j L) + \cos(\eta_j L))/(\sinh(\eta_j L) + \sin(\eta_j L)) \tag{A13}$$

Note that the constraint force λ is expanded into a modal series as are u and w. Also note that for the linear case, only the zeroth mode is needed for λ, i.e., $k = 0$, and λ is constant with respect to both x and t. For the nonlinear case, λ varies with x and t.

These mode shapes are all normalized such that the length variable ξ runs from 0 to 1 and the endpoints of the modal functions are 1, 0, or −1 depending on the geometric constraints.

From previous work [24], the system of governing equations which describes the unforced ($Q_n = 0$), undamped cantilevered beam motion is as follows:

$$0 = m\int_0^L \Psi_i^u \Psi_i^u \, dx \, \ddot{u}_i - \sum_k \lambda_k \int_0^L \Psi_i^{u\prime} \Psi_k^{\lambda} \, dx \tag{A14}$$

$$0 = m\int_0^L \Psi_j^w \Psi_j^w \, dx \, \ddot{w}_j + \boldsymbol{\omega}_j^2 m \int_0^L \Psi_j^w \Psi_j^w \, dx \, w_j - \sum_k \sum_{j1} \lambda_k w_{j1} \int_0^L \Psi_k^{\lambda} \Psi_{j1}^{w\prime} \Psi_j^{w\prime} \, dx + EI \sum_{j1}\sum_{j2}\sum_{j3} \int_0^L (\Psi_{j1}^{w\prime\prime} \Psi_{j2}^{w\prime\prime} \Psi_{j3}^{w\prime} \Psi_j^{w\prime} + \Psi_{j1}^{w\prime\prime} \Psi_{j2}^{w\prime} \Psi_{j3}^{w\prime} \Psi_j^{w\prime\prime}) \times dx \, w_{j1} w_{j2} w_{j3} \tag{A15}$$

$$0 = \sum_i u_i \int_0^L \Psi_k^{\lambda} \Psi_i^{u\prime} \, dx + \frac{1}{2}\sum_{j1}\sum_{j2} w_{j1} w_{j2} \int_0^L \Psi_k^{\lambda} \Psi_{j1}^{w\prime} \Psi_{j2}^{w\prime} \, dx \tag{A16}$$

As before [24], normalizing the modal coefficients u_i and w_j and normalizing the integral terms such that the integration is from 0 to 1 with respect to $x/L \equiv \xi$ produces several useful definitions. Index notation for the one-dimensional vectors and the two-dimensional matrices can be rewritten in boldface matrix notation as indicated after the right arrows. However, the three- and four-dimensional tensors will be left in index form to avoid the introduction of tensor notation

$$\overline{u}_i \equiv \frac{u_i}{L} \Rightarrow \mathbf{u}, \quad \overline{w}_j \equiv \frac{w_j}{L} \Rightarrow \mathbf{w}, \quad \lambda_k \Rightarrow \lambda, \quad \boldsymbol{\omega}_j^2 \Rightarrow \boldsymbol{\omega}^2$$

$$M_{ii}^u \equiv \int_0^1 \Psi_i^u \Psi_i^u \, d\xi \Rightarrow \mathbf{M_u}, \quad M_{jj}^w \equiv \int_0^1 \Psi_j^w \Psi_j^w \, d\xi \Rightarrow \mathbf{M_w}$$

$$A_{ik} \equiv \int_0^1 \Psi_i^{u\prime} \Psi_k^{\lambda} \, d\xi \Rightarrow \mathbf{A}, \quad B_{kj_1j} \equiv \int_0^1 \Psi_k^{\lambda} \Psi_{j_1}^{w\prime} \Psi_j^{w\prime} \, d\xi$$

$$P_{j_1j_2j_3j} \equiv \int_0^1 \left(\Psi_{j_1}^{w\prime\prime} \Psi_{j_2}^{w\prime\prime} \Psi_{j_3}^{w\prime} \Psi_j^{w\prime} + \Psi_{j_1}^{w\prime\prime} \Psi_{j_2}^{w\prime} \Psi_{j_3}^{w\prime} \Psi_j^{w\prime\prime}\right) d\xi$$

A discussion on vector/matrix size and characteristics may be appropriate. Vectors $\mathbf{u}$, $\mathbf{w}$, and $\boldsymbol{\lambda}$ are length I, J, and K, respectively. Matrices $\mathbf{M_u}$ and $\mathbf{M_w}$ are diagonal matrices of size I^2 and J^2, respectively. Matrix $\mathbf{A}$ is of size $\mathrm{I} \times \mathrm{K}$. Tensor $\mathbf{B}$ is three-dimensional of size $K \times \mathrm{J} \times \mathrm{J}$, and $\mathbf{P}$ is four-dimensional of size J^4. Matrix $\boldsymbol{\omega}^2$ is a diagonal matrix with each nonzero entry as the square of the corresponding modal natural frequency.

The final two terms in Eq. (A15) are tensor summations which simplify to vectors of length J, and the final term in Eq. (A16) is a tensor summation which simplifies to a vector of length K. These may be represented in their final vector form as follows:

$$\{\mathbf{Pw}^3\} = \sum_{j_1}\sum_{j_2}\sum_{j_3} L^{-2} EI \, P_{j_1j_2j_3:} \overline{w}_{j_1} \overline{w}_{j_2} \overline{w}_{j_3}$$

$$\{\mathbf{Bw\lambda}\} = \sum_k \sum_{j_1} B_{kj_1:} \overline{w}_{j_1} \lambda_k$$

$$\{\mathbf{Bww}\} = \sum_{j_1}\sum_{j_2} B_{:j_1j_2} \overline{w}_{j_1} \overline{w}_{j_2}$$

The unforced and undamped normalized system of equations is as follows:

$$0 = L^2 m \mathbf{M_u} \ddot{\mathbf{u}} - \mathbf{A}\boldsymbol{\lambda} \tag{A17}$$

$$0 = L^2 m \mathbf{M_w} \ddot{\mathbf{w}} + L^2 m \boldsymbol{\omega}^2 \mathbf{M_w} \mathbf{w} + L^{-2} EI \{\mathbf{Pw}^3\} - \{\mathbf{Bw\lambda}\} \tag{A18}$$

$$0 = \mathbf{A}^{\mathrm{T}}\mathbf{u} + \frac{1}{2}\{\mathbf{Bww}\} \tag{A19}$$

References

[1] Beck, M., 1952, "Die Knicklast Des Einseitig Eingespannten, tangential Gedrückten Stabes," Z. Angew. Math. Phys., **3**(3), pp. 225–228.

[2] Bolotin, V., 1963, *Nonconservative Problems of the Theory of Elastic Stability*, Pergamon Press, Oxford, UK.

[3] Bolotin, V., and Zhinzher, N., 1969, "Effects of Damping on Stability of Elastic Systems Subjected to Nonconservative Forces," Int. J. Solids Struct., **5**(9), pp. 965–989.

[4] Chen, M., 1987, "Hopf Bifurcation in Beck's Problem," Nonlinear Anal., Theory, Methods Appl., **11**(9), pp. 1061–1073.

[5] Di Egidio, A., Luongo, A., and Paolone, A., 2007, "Linear and Non-Linear Interactions Between Static and Dynamic Bifurcations of Damped Planar Beams," Int. J. Non-Linear Mech., **42**(1), pp. 88–98.

[6] Luongo, A., and Di Egidio, A., 2005, "Bifurcation Equations Through Multiple-Scales Analysis for a Continuous Model of a Planar Beam," Nonlinear Dyn., **41**(1–3), pp. 171–190.

[7] Luongo, A., and Di Egidio, A., 2006, "Divergence, HOPF and Double-Zero Bifurcations of a Nonlinear Planar Beam," Comput. Struct., **84**(24–25), pp. 1596–1605.

[8] Luongo, A., and D'Annibale, F., 2017, "Nonlinear Hysteretic Damping Effects on the Post-Critical Behaviour of the Visco-Elastic Beck's Beam," Math. Mech. Solids, **22**(6), pp. 1347–1365.

[9] Stanciulescu, I., Virgin, L., and Laursen, T., 2007, "Slender Solar Sail Booms: Finite Element Analysis," J. Spacecr. Rockets, **44**(3), pp. 528–537.

[10] Langthjem, M., and Sugiyama, Y., 2000, "Dynamic Stability of Columns Subjected to Follwer Loads: A Survey," J. Sound Vib., **238**(5), pp. 809–851.

[11] Ziegler, H., 1952, "Die Stabilitätskriterien Der Elastomechanik," Ing.-Arch., **20**(1), pp. 49–56.
[12] Luongo, A., and D'Annibale, F., 2014, "On the Destabilizing Effect of Damping on Discrete and Continuous Circulatory Systems," J. Sound Vib., **333**(24), pp. 6723–6741.
[13] Hagedorn, P., 1970, "On the Destabilizing Effect of Non-Linear Damping in Non-Conservative Systems With Follower Forces," Int. J. Non-Linear Mech., **5**(2), pp. 341–358.
[14] Thomson, J., 1995, "Chaotic Dynamics of the Partially Follower-Loaded Elastic Double Pendulum," J. Sound Vib., **188**(3), pp. 385–405.
[15] Crespo da Silva, M. R. M., 1978, "Harmonic Non-Linear Response of Beck's Column to a Lateral Excitation," Int. J. Solids Struct., **14**(12), pp. 987–997.
[16] Crespo da Silva, M., 1978, "Flexural-Flexural Oscillations of Beck's Column Subjected to a Planar Harmonic Excitation," J. Sound Vib., **60**(1), pp. 133–144.
[17] Luongo, A., and D'Annibale, F., 2013, "Double Zero Bifurcation of Non-Linear Viscoelastic Beams Under Conservative and Non-Conservative Loads," Int. J. Non-Linear Mech., **55**(Suppl. C), pp. 128–139.
[18] D'Annibale, F., Ferretti, M., and Luongo, A., 2016, "Improving the Linear Stability of the Beck's Beam by Added Dashpots," Int. J. Mech. Sci., **110**, pp. 151–159.
[19] Crespo da Silva, M., and Glynn, C., 1978, "Non-Linear Flexural-Flexural-Torsional Dynamics of Inextensional Beams—I: Equations of Motion," J. Struct. Mech., **6**(4), pp. 437–448.
[20] Crespo da Silva, M., and Glynn, C., 1978, "Non-Linear Flexural-Flexural-Torsional Dynamics of Inextensional Beams—II: Forced Motions," J. Struct. Mech., **6**(4), pp. 449–461.
[21] Dowell, E., and McHugh, K., 2016, "Equations of Motion for an Inextensible Beam Undergoing Large Deflections," ASME J. Appl. Mech., **83**(5), p. 051007.
[22] Hamdan, M., and Dado, M., 1997, "Large Amplitude Free Vibrations of a Uniform Cantilever Beam Carrying an Intermediate Lumped Mass and Rotary Inertia," J. Sound Vib., **206**(2), pp. 151–168.
[23] Mahmoodi, S. N., Jalili, N., and Khadem, S. E., 2008, "An Experimental Investigation of Nonlinear Vibration and Frequency Response Analysis of Cantilever Viscoelastic Beams," J. Sound Vib., **311**(3–5), pp. 1409–1419.
[24] McHugh, K., and Dowell, E., 2018, "Nonlinear Responses of Inextensible Cantilever and Free-Free Beams Undergoing Large Deflections," ASME J. Appl. Mech., **85**(5), p. 051008.
[25] Raviv Sayag, M., and Dowell, E., 2016, "Linear Versus Nonlinear Response of a Cantilevered Beam Under Harmonic Base Excitation: Theory and Experiment," ASME J. Appl. Mech., **83**(10), p. 101002.
[26] Tang, D., Zhao, M., and Dowell, E., 2014, "Inextensible Beam and Plate Theory: Computational Analysis and Comparison With Experiment," ASME J. Appl. Mech., **81**(6), p. 061009.
[27] Villanueva, L., Karabalin, R. B., Matheny, M. H., Chi, D., Sader, J., and Roukes, M., 2013, "Nonlinearity in Nanomechanical Cantilevers," Phys. Rev. B, **87**(2), p. 024304.
[28] Novozhilov, V., 1953, *Foundations of the Nonlinear Theory of Elasticity*, Graylock Press, Rochester, NY.
[29] Tang, D., Gibbs, S., and Dowell, E., 2015, "Nonlinear Aeroelastic Analysis With Inextensible Plate Theory Including Correlation With Experiment," AIAA J., **53**(5), pp. 1299–1308.
[30] Kirillov, O. N., and Seyranian, A. O., 2005, "The Effect of Small Internal and External Damping on the Stability of Distributed Non-conservative Systems," J. Appl. Math. Mech., **69**(4), pp. 529–552.